

We are IntechOpen, the world's leading publisher of Open Access books Built by scientists, for scientists

4,800

Open access books available

122,000

International authors and editors

135M

Downloads

Our authors are among the

154

Countries delivered to

TOP 1%

most cited scientists

12.2%

Contributors from top 500 universities



WEB OF SCIENCE™

Selection of our books indexed in the Book Citation Index
in Web of Science™ Core Collection (BKCI)

Interested in publishing with us?
Contact book.department@intechopen.com

Numbers displayed above are based on latest data collected.
For more information visit www.intechopen.com



The Translatory Wave Model for Landslides

Jónas Eliásson and Þorsteinn Sæmundsson

Abstract

The Saint-Venant equations are usually the basis of numerical models for landslide flows. They are nonstationary and nonlinear. The theory for translatory waves in a prismatic channel and a funneling channel can be used for landslides using the assumption of either turbulent or laminar flow in the slide. The mathematics of translatory waves traveling over dry land or superimposed on another flow are developed. This results in a new slope factor controlling the flow velocity, together with the Chezy coefficient used in previous applications of the translatory wave theory. Flow times for the slide to reach a given destination, slide depth, and velocity can be calculated using the initial magnitude of the flow in the slide. The instabilities of the wave tail are discussed. Three case studies are presented: a submarine slide that started the Tohoku tsunami in Japan, the Morsárjökull rock avalanche in SE Iceland, and the Móafellshyrna slide in central N Iceland.

Keywords: landslide model, translatory wave, landslides, rock avalanche, debris slides, Iceland

1. Introduction

Landslides are a natural phenomenon that more often than not can be described as an environmental disaster. Landslides are responsible for countless human lives, and there is no remedy against their occurrence. The only way to counteract the danger is preparedness, knowing the danger, assessing the hazard, operating a warning system, and keeping people out of the way of the slides, a task all governments and rescue services, civil and military, deal with every day.

Landslides are very different in character, so in the civil protection work, everything matters, area, weather, soil, topography, surface structure, and what triggers the slide. Consequently, the classification system for landslides is very complicated. A very good overview of the modern trend of classification can be found in [1] where types of landslides are discussed separately. A quick overview on what this classification is all about can be found in the course material in [2], where classification systems from 1938, 1958, and 1978 are listed plus a unified classification system.

The classification has to take into account all the danger factors previously mentioned and is therefore quite complicated and in constant development, and a lot has happened since it appeared. For instance, today statistical methods are used to assess the danger [3], and sometimes they bring about scaling laws known from

the fractal theory [4]. The statistical methods have not found their way into the classification system.

One of the largest uncertainties and in many instances the very reason for the use of statistics in the science of landslides is the instability problem. Instability can trigger a landslide quite suddenly, and then again, small cracks may be discovered, and they keep widening for a long time; it is quite evident that a landslide will occur at some time, but there is no way to tell when it happens.

Instability problems are well known in soil mechanics, e.g., liquefaction and wave formation in hydrodynamics. Both can be triggered by an external force like earthquake. A lot of research effort is devoted to the problem of landslide triggering [5], sometimes with stochastic input routines [6, 7] and others with models describing the aftermath, for hazard assessment [8], or modeling of the flow of the slide itself [9], sometimes with assistance of remote sensing data [10].

Landslide models can be numerical or analytical. Both are very dependent of the boundary conditions. Both need a physical basis to describe the dynamics of the slide, especially the particle velocity. The simplest, but very efficient, method is to put the velocity proportional to the gradient of the elevation of the surface on the one hand and to the shear force in excess of the shear strength of the soil on the another. An example of the mathematical formulation this assumption leads to is Eqs. 1 and 2 in [5]. The basis of this approach is Newton's law of viscosity.

A necessary condition for this approach to hold is that the inertial terms, other than acceleration, in the full flow equation system can be neglected. This means that all nonlinear terms can be left out. This will be the case for many types of landslides, due to the high viscosity in them. However, many slides will be running faster than that, and they are the most dangerous ones.

In the following we shall discuss the translatory wave landslide model. This model can be used for the front of the landslide, the velocity of it, and how far it flows. The criterion for using the model is that the slide has to be flowing in a regular manner, not just a fall of soil or rock fragment down a steep slope, so many of the types defined in the classification systems and discussions of different types mentioned above will be excluded from this approach. For the others, i.e., regular slides that do actually flow, the translatory theory can in most cases be used.

The translatory model involves analyses that are complicated in nature but lead to a simple system when fully derived. It can be very useful in studies one has to do prior to numerical model studies in defining the area, extent of boundaries, and limits to the various parameters involved. Thus, it can save a lot of trial and error work in constructing the model and elimination of numerical instabilities. And sometimes it produces results that are good enough as demonstrated in the case studies.

2. Theoretical considerations

2.1 Theory of translatory waves

A translatory wave runs down a channel slope with flow that is not constant in time but varies slowly. In treatment of such flow, it is natural to look for waves of fixed shape progressing down a channel. Such waves in shallow water have been investigated earlier; a further treatment is presented in [11] using Chezy's equation for the flow resistance instead of the more complicated Manning's equation. This simplifies the mathematics of the problem. The starting point is the continuity and momentum equations for an arbitrary prismatic channel. For the sake of simplicity, only two cases are treated, that of a wide rectangular inclining flume and a rectangular inclining funnel.

2.2 Translatory waves in a flume

2.2.1 The translatory wave

The equations of Saint-Venant describing flow down an inclining plane can be taken from many textbooks on fluid mechanics or hydrology; they are

$$\text{Equation of continuity: } \frac{\delta y}{\delta x} + \frac{\partial q}{\partial x} = 0 \quad q = yv \quad (1)$$

$$\text{Momentum eq.: } \frac{\delta v}{\delta t} + v \frac{\partial v}{\partial x} + g \frac{\partial v}{\partial x} (I - I_0) = 0 \quad (2)$$

where:

y water depth

q channel flow per unit width

v velocity

x streamwise coordinate

t time

g acceleration of gravity

I friction slope

I_0 channel slope

The system obviously admits a solution where $v = v(x - ct)$ and $y = y(x - ct)$ with c as the constant wave celerity. The momentum equation degenerates to

$$\frac{dy}{d\xi} + \frac{c^2}{C^2 g y} = I_0 \quad c^2 = C^2 g I y \quad (3)$$

where C is the nondimensional Chezy constant and $\xi = x - ct$. This equation can readily be integrated.

$$\frac{y}{y_0} + \ln \left(1 - \frac{y}{y_0} \right) = I_0 \frac{x - ct}{y_0}; \quad y_0 = 0; \quad x - ct \leq 0 \quad (4)$$

This is the form of the approaching wave. The wave passes the origin at time zero: $x = t = 0 \Rightarrow y = 0$.

It is easily seen that the wave will continue to run if $I > 0$, i.e., the flow will not stop until the surface has become horizontal. This means that the landslide is of liquefied, or fluidized, soil. This means that the water content of the slide is rather high. This does not have to be the case. The slide's material may very well have finite shear strength. Then it stops at a finite slope.

As time progresses y approaches the normal depth y_0 , while the discharge q approaches the value

$$q_0 = c y_0 = C \sqrt{g I_0} y_0^{3/2} \quad (5)$$

from which the normal depth y_0 and c can be calculated if q_0 is known. Equation (4) can also be used for landslides, as will be demonstrated.

2.2.2 Basic fluid mechanics of landslide flows

Call the shear stress τ and the pressure on the bottom (normal stress) σ in uniform flow of a soil in a landslide down a plane inclined by an angle θ to the

horizontal, and let y' be the distance from the bottom and y the total depth. Then we have from any textbook in hydraulics

$$\tau = \rho g \sin \theta (y - y'); \quad \sigma = \rho g \cos \theta (y - y'); \quad \rightarrow \quad \tau/\sigma = \tan \theta \quad (6)$$

If the shear resistance of the soil is purely frictional with friction angle φ , there is no flow for $\varphi > \Theta$. For cohesive soils this is a little more complicated. Motion starts when $\tau \geq \sigma \tan \varphi + c'$, where c' is the cohesion. In the no flow situation, the cohesion can be a substantial part of the total shear strength of the soil; however, the cohesion is not a material constant for the soil; upon deformation and start of flow, c' is reduced, and after that we can approximate the shear strength of the soil with a dynamical friction angle φ' and a zero cohesion. Then we will have $\varphi' < \Theta$ as condition for flow. This means that the slide will stop when it flows on a slope $\Theta < \varphi'$, and then the shear stress ratio is $\tau_{cr}/\sigma = \tan \varphi'$, which is the critical shear stress ratio. The shear stress in excess of the critical τ_{cr} is then

$$(\tau - \tau_{cr})/\sigma = \tan \theta - \tan \varphi'; \quad \rightarrow \quad \tau - \tau_{cr} = \rho g \sin \theta (1 - \tan \varphi' / \tan \theta) (y - y') \quad (7)$$

This can be combined with Newton's law of viscosity.

$$(\tau - \tau_{cr})/\rho = g \sin \theta (y - y') (1 - \tan \varphi' / \tan \theta) = C_f \frac{dv}{dy'} \quad (8)$$

$$\text{Here we have: } \begin{cases} \text{Laminar flow: } C_f = \text{kinematic viscosity} \\ \text{Turbulent flow: } C_f = \text{eddy viscosity} \end{cases} \quad (9)$$

Kinematic viscosity is normally assumed constant, but eddy viscosity changes with the distance from the wall in accordance with Prandtl's theory of wall turbulence. This makes the difference that the velocity profile will be parabolic in the laminar case and the maximum velocity in a fixed distance in the flow path, i.e., $v_{max} = 1.5 v_{average}$ for a fixed x in (4). In the turbulent case, v_{max} is closer to $v_{average}$ than that.

Combining this with (4) and (5), we put $c = v_{av}$, and the flow becomes $q = c y$. The actual variation of the velocity with y' will for all practical purposes affect the wave form (4) only slightly when the celerity in the landslide is $c \ll \sqrt{gy}$ which is the celerity of the surface gravity wave.

Equations (8) and (9) are similar to those for ordinary channel flow except (6) is multiplied by $(1 - \tan \varphi' / \tan \theta)$ to get (8), which gives the excess shear stress or the resistance to the flow. Then (9) provides the relation to the velocity through the unknown resistance coefficient C_f . In the laminar case, it is assumed constant, and then we have a flow proportional to the slope, which in a free landscape gives a flow in the direction of the elevation gradient. This is a popular idea for landslide model (see, e.g., [6, 7]).

C_f does not need to be constant, it can depend on the velocity, giving a turbulence-like flow resistance. A simple way to include this possibility is to use Chezy's coefficient defined as

$$c = v_{av} = C \sqrt{(\tau - \tau_{cr})/\rho} = C \sqrt{gy \sin \theta (1 - \tan \varphi' / \tan \theta)} \quad (10)$$

C is not a constant as originally proposed by Chezy but a slowly varying implicit function of the velocity and is thus constant while c is constant. To get an idea about the variation of C with the resistance factor in turbulent flows, one can study Section 15.2 in [12]. There is an implicit relation proposed by ASCE in 1963; it is

based on a large volume of experimental data. For low velocity flows, it gives laminar friction. Our implicit relation would have to possess that property too, but otherwise it remains unknown until sufficient experimental data for landslides is available.

Example 1.

We call $S_f = \sin\Theta (1 - \tan\phi'/\tan\Theta)$ the slope factor. It can be found in other models; see, e.g., (5) in [8]. We take the value 0.5. and list in **Table 1** corresponding C values for various slides, calculated from (10).

C is proportional with the velocity but varies much more slowly with y . It is therefore a possibility that approximate average regional values for C can exist in regions with similar geological settings. C for other slope factors S_f can easily be found in **Table 1** by multiplying the C values with $a = \sqrt{(0.5/S_f)}$.

2.2.3 Properties of the slide function

When C is known, we can turn back to (4) and modify it to fit a slide where the flow resistance is the excess shear stress. In Section 2.3.1, we defined the slope factor for uniform flow from the Chezy coefficient C and the bottom slope. Now C is defined in the same way but for local surface slope S_f , not bottom slope S_{f0} . With $\xi = x - ct$ as before, the local velocity will be

$$c = C \sqrt{gy \sin \theta \frac{dy}{d\xi} (1 - \tan \phi' / \tan \theta)} = C \sqrt{gy S_f} \quad (11)$$

And (4) is modified to

$$\frac{y}{y_0} + \ln \left(1 - \frac{y}{y_0} \right) = S_{f0} \frac{x - ct}{y_0}; \quad y_0 = 0; \quad x - ct \leq 0 \quad (12)$$

The mathematical properties of Eq. (11) are discussed in [11] and the function plotted in **Figure 1** in [12].

It is obvious from (11) that y approaches y_0 very fast with time. According to (4) the flood reaches a depth that is 90% of y_0 in $x = 0$ in time $t = 1.4 y_0 / (S_{f0} c)$. This is only a few minutes according to the values in **Table 1**; the slower the slide, the steeper is the front of the approaching slide.

The flow q_0 in m^3/s per m width in the slide is found by modifying (5) to (12):

y/c	0.5	1	2	3
1	0.22	0.45	0.89	1.34
2	0.16	0.32	0.63	0.95
3	0.13	0.26	0.52	0.77
4	0.11	0.22	0.45	0.67
5	0.10	0.20	0.40	0.60
6	0.09	0.18	0.37	0.55
7	0.08	0.17	0.34	0.51
8	0.08	0.16	0.32	0.47

Table 1.
 C for y in m , c in m/s , and slope factor 0.5.

$$q_0 = cy_0 = C\sqrt{gS_{f0}}y_0^{3/2} \quad (13)$$

2.2.4 Change of slope or channel form

If the slope changes, the velocity will adjust to a new depth and velocities in a region just before and just after the slope change as long as the flow is subcritical in the fluid mechanical sense. When the slide flows downhill, the slope will in most cases be diminished. The flow will adapt to the new depth on a short distance.

Equation (5) can be used to find the new depth by using the fact that the flow is the same, upstream and downstream of the slope change. The same approach is used if the channel changes form.

2.2.5 Flow in a funnel-shaped flume

The continuity equation in a channel shaped as a funnel flume is

$$\frac{\partial y}{\partial t} + \frac{1}{r} \frac{\partial(rq)}{\partial r} = 0; \quad q = yv \quad (14)$$

Here we shall only consider the translatory wave when the wave celerity is equal to the water velocity ($v = c$) and the momentum equation degenerates to the form (3). In this case we get a direct solution. But as the flow spreads out, the equilibrium between surface slope and bed slope will come even quicker than before. We can therefore assume the kinematic wave equation to be valid, a few minutes after the front has passed. The kinematic wave routing equation (valid when changes in velocity head are small) reads [11]

$$\frac{\partial Q}{\partial t} + c \frac{\partial Q}{\partial r} = d \frac{\partial^2 Q}{\partial r^2}; \quad d = \frac{q}{2S_{f0}} \quad (15)$$

Using $Q = Q(r - ct)$ as before cancels the left-hand terms, and we get the expression $Q = \alpha r y v$ where α is the opening angle of the funnel.

$$Q = C_1(r - ct) + C_2 \quad \text{or} \quad y = (a(r - ct) + b)/r \quad (16)$$

In (15) a and b are unknown constants. They are needed because Eq. 11 cannot fulfill the boundary condition $Q = 0$ when $r - ct = 0$. Equation 11 is valid with sufficient

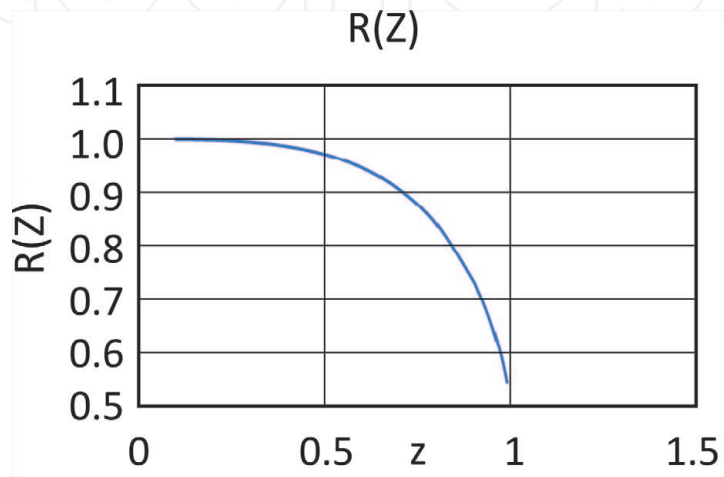


Figure 1.
Chart of the R(Z).

accuracy after y has reached 90 % of y_0 or more. Many natural channels have a shape that can be approximated as a series of flumes with constant width and slowly changing funnels. It is therefore quite clear that a translatory wave can flow down any channel, adapt to the changing environment, and still be a translatory wave.

3. Limitations of the theory

3.1 Limitations of the translatory model

The most severe limitation of the translatory model is the very heart of the theory, the progressive wave. The wave starts at some point; for a while there will be either increasing or diminishing flow in this point. While we have increasing or constant flow, we are in the head of the wave. For constant flow (11) and (12) apply, but a flow increase will come as a new translatory wave riding upon the first [11], but (11) will apply, with local y and S_f instead of y_0 and S_{f0} .

3.2 The recessing translatory wave

3.2.1 The recessing wave and the flow head

Diminishing flow is more complicated. Then we are in the tail of the wave head, the wave is recessing, and it is no longer progressing with a constant speed. If it is necessary to calculate this flow, numerical simulation using the full Saint-Venant equations, modified according to Section 2.2.3, may be tried. This involves more advanced programming than for a water waves and has not been tried for landslides using nonlinear friction. In [13] a very advanced model of this kind is presented, using linear friction, but allowing different rheologies, both viscous and non-Newtonian flow, which should give the same possibilities, as nonlinear friction coupled with a slope factor can be used as a tool to imitate non-Newtonian behavior.

The head of the wave is the most damaging part, and the head also determines the length of the damaged area. Therefore, the head flow is the most important, and the flow in the tail is not as interesting in disaster prevention studies.

3.2.2 The laminar wave

If it is clear from the beginning that the velocity is low enough, so all inertial and nonlinear terms can be neglected, and the gradient flow model can be applied in a way like [6, 7]. Using a notation similar to theirs, but using Δy instead of ΔH (with Δ meaning the gradient/divergence operator), we would have a slope factor as in Example 1 and (10).

$$S_f = \sin \theta (1 - \tan \phi' / \tan \theta) = \sin \theta (1 - |\Delta y / (|\tan \theta|)|) \quad (17)$$

Θ is the bottom slope in the direction of the flow. Using the laminar model from (8) and (9), flow equations will be

$$\bar{q} = \bar{v}y = 2 / (3C_f) S_f y^3 \Delta y / |\Delta y| \quad \frac{\partial y}{\partial t} = \Delta \bar{q} \quad (18)$$

$$\frac{\partial y}{\partial t} = \Delta (2 / (3C_f) S_f y^3 \Delta y / |\Delta y|) \quad (19)$$

There are several ways to linearize (18), either piecewise or totally, and use it to find the flow and the slide area. This is probably the most popular slide model, but it

demands a linear relationship between the flow resistance ($\tau - \tau_{cr}$) in (8) and the surface gradient.

4. The onset of motion

4.1 The initial state

4.1.1 Development of instability

Instability occurs when the shear stress in the soil becomes larger than the critical strength, then a landslide may start. The causes of this can be geological, morphological, physical, or human (see [1] or [2]) or any combination of these causes. A misjudgment of the geological or morphological conditions of the site where a slope is being constructed, or altered, may lead to a landslide. This would be listed as a human cause but can have the simple physical reason that the soil could not withstand the stress increase imposed by the construction work.

Instability of this kind can take time to develop. The soil may grow thicker by time, a bulge can develop due to swelling where the horizontal stress is at its maximum, and a slide will start when the horizontal stress exceeds the passive pressure limit. During the following plastic deformation of the soil, the cohesive strength (c') of the soil is diminished, the plastic deformation is accelerated, the instability has set in, and we have the landslide running possibly a debris flow.

The instability can also set in because c' is reduced by water uptake of the soil, either by infiltration from increased groundwater pressure or soaking of the soil by rain. This reduces the φ' at once and sets in the instability when we have $\varphi' < \theta$.

A regional study of slopes and lithology, and analysis together with other factors, can bring about important statistics concerning landslide susceptibility and probability of occurrence of landslides caused by the above described instability [3]. This may even be done globally using satellite data [10]. Predicting the timing and location of landslide initiated by developing instability of this kind is very difficult, but considerable success is reported in this field [5, 9].

4.1.2 Slope instability by external causes

External forces can cause slope failure that starts a landslide. These are earthquakes, other tectonic movements, and explosions that rupture the soil and reduce the shear strength of the soil by one quick movement. An instability of this kind depends on the strength of the external force and is even more difficult to predict.

Large earthquakes usually start landslides, both on land and in the sea (submarine slides).

There may be any combination of events that cause landslides. A landslide due to developing instability may be triggered by a small earth tremor. This will cause the landslide to happen sooner than otherwise expected.

5. Practical aspects of the translatory model

5.1 The estimation and use of the Chezy coefficient

The translatory model is based on the Chezy coefficient that can be relatively stable regionally, but this must be established by extensive field investigations.

In field investigations of actual slides, it may be difficult to find the actual investigations begin after the slide stops. Then the total flow of the slide is an important factor. In a point where we have

$$Z = y/y_0 \quad \text{and} \quad L = -x/y_0 \quad (20)$$

consider Eq. (11) at time $t = 0$; the tip of the slide is in $x = 0$. Let $x < 0$ be any position, and the relation for the dimensionless total flow past it is

$$Q^* = ZL - R(Z)/S_f; \quad R(Z) = \left(1 + (1 + Z)^2\right) - (1 - Z) \ln(1 - Z) \quad (21)$$

From this we deduce

$$S_f = R(Z)/(ZL - Q^*). \quad (22)$$

The dimensional value of Q is $Q = Q^*y_0^2$. When Q is found from field investigations, (20) is a rather robust formula to find S_f . As seen from **Figure 1**, Z does not vary very much except in the range $0.5y_0 < y < 0.9y_0$. Outside this range we have 1 or 0.5 for $R(Z)$. If $R(Z)$ is estimated to be 0,5–0,6, we are in the Z range $0.9 < y/y_0 < 1$.

This gives the possibility to use an estimated y_0 value in (20) and find S_f .

Example 1 shows how S_f relates to the hillslope $\tan\theta$ and the critical shear stress ratio $\tan\phi'$ that also relates to the soil parameters.

To find the Chezy coefficient C , there must be some observations of flow times. If the time t_x that it took the slide to move from $-x$ in (19) to $x = 0$, we simply have $c = x/t_x$. Then (12) gives an estimate for C .

But even without an estimate for C , the estimate for y_0 and (11) give us an estimate of how large an area a slide with a known total mass will cover.

5.2 Discussion of the method

As stated in the introduction, the translatory theory can be used for any landslide flowing in a regular manner, which means that the bottom friction and bed slope control the flow. The velocity of vertical falls, turfs, frozen blocks of soil, ice, or snow is not governed by the friction in the flowing phase only at the onset of motion and when the sliding stops. At high velocities a lot of air can be mixed into the flow; this is especially true for avalanches of dry fine-grained snow. In such cases material properties such as density and viscosity may become indeterminable.

For flowing slides, the translatory wave theory can be used for any event, debris flows, or mudflows. In [5–8] slides that this theory can be used for are discussed. But it is also possible to apply it for unusual cases as submarine slides and rock avalanches as will be demonstrated in the next chapter.

The main application of the translatory theory is to use the information available of source area material properties and magnitudes, rundown slopes, and flow depths to estimate the flow coefficients S_f and C . A good database for these coefficients will make it possible to estimate them at sites where a slide danger has been identified and the slide is expected to fall anytime.

In such cases a danger area has to be estimated for use by the civil protection authorities. They can declare the area off limits (all visits forbidden), close roads, and order areas to be evacuated. It is especially in the case of evacuations and closing roads for all traffic that an overcautious and too large a danger area estimate can come under severe criticism.

When the size of a danger area is estimated, there has to be a safety margin. In construction it is decided by the safety margin to put on material strength and design loads. Using S_f and C to find a danger area, the safety margin can be decided in the same way. The most likely values for S_f and C have to be found first and the safe values to be used in the estimation decided afterwards.

6. Case studies

6.1 Case study 1: the Tohoku submarine slide

6.1.1 Location and event

The most famous tsunami event of recent years hit Honshu, the big island in Japan, on Friday 11 March 2011 at 05:46 UTC. Its location was off the Pacific coast of Tohoku, Japan. The earthquake event and the devastation caused by this tsunami is very well documented; here we shall follow [14].

The cause was a M_w 9.0 (magnitude moment) undersea megathrust earthquake. The epicenter was approximately 70 km east of the Oshika Peninsula of Tohoku with the hypocenter in approximately 30 km deep water.

As most earthquakes above M_w 7.0 do, it caused a tsunami. The tsunami was much bigger than what could be expected and caused a massive devastation. Tens of thousands of people suffered loss of life or all their possessions. Houses and other structures were swept away from large areas. The town of Sendai was very badly hit and 13 other Japanese cities.

The most serious incident, however, was a meltdown in the Fukushima Daiichi Nuclear Power Plant, when the tsunami proved too high for the coastal defenses and flooded the emergency generators.

6.1.2 Properties and data

In [14] it is suggested that the bottom deformations that caused the very strong Tohoku tsunami in the Pacific Ocean can be explained by a submarine landslide. This suggests that the coseismic slip of the earthquake triggers a sliding of the surface sediments. In combination they cause the bottom deformation.

Finally, it can thus be concluded that the coseismic slip and the landslide are both responsible for the Tohoku tsunami in March 2011, not the coseismic slip alone.

From the data obtained in the exploratory drilling at the site shown in Figure 2 in Ref. [14], it was concluded that the tsunami was caused by the mass movement shown in Figure 3 in Ref. [14]. The slide triggered by the earthquake amplifies the tsunami.

This landslide is not very high compared to what has happened elsewhere. But it is quite possible that the coastal defenses of Fukushima would have saved the emergency generators and prevented the nuclear disaster had the landslide not happened.

The main data for the slide were originally deduced from [16–18]. In [14] we find the following:

Bottom slope is 9 %, $c = 2$ m/s, and $y_0 = 8$ m. The length of the slide is 117.5 km, the width of the slide is 110 km, but the length of the flow path is only 60 m, and the flow time is thus 30 s. The volume moved by the slide is 96.8 km^3 .

6.1.3 Evaluation

Using **Table 1** and the bottom slope, we find a C value of 0.32. Corrected for $S_f \approx 0.1$, we get the value of the Chezy coefficient $C = 0.71$.

This shows that in assessing the tsunami risk in the Pacific coastal regions of Japan, the landslide risk must be considered. This fact may result in that considerably larger events than the Tohoku tsunami are possible if a larger slide than this 8-m-thick slide is released.

The assessment of this possibility of larger slides can be difficult; there is considerable uncertainty in estimating the height (y_0) of possible landslide, but this may be done using drilled exploration wells, like the one shown in Figure 2 in Ref. [14]. The flow time will be the estimated duration of the earthquake, so using the C found here, there may be a possibility to estimate the volume moved by a slide using (20)–(21) and thereby the strength of the corresponding tsunami.

6.2 Case study 2: the rock avalanche on the Morsárjökull outlet glacier, SE Iceland

6.2.1 Location and event

On March 20, 2007, a large rock avalanche fell on the Morsárjökull outlet glacier, in the southern part of the Vatnajökull ice cap, in Southeast Iceland (**Figure 2**). This rock avalanche is considered to be one of the largest rock avalanches which have occurred in Iceland during the last decades [19].

The Morsárjökull glacier is a small outlet glacier on the southern side of the Vatnajökull ice cap in Southeastern Iceland, located between the Þorsteinshöfði Mountain (1343 m) and Skarðatindur Mountain (1385 m) to the east and the Austurhnúta peak (1084 m) in the Miðfell Mountain (1430 m) to the west (**Figure 2**). The glacier is about 4 km long and 750–900 m wide in the uppermost part and around 800–900 wide in the lower part. Its surface is around 3.3 km². The glacier is surrounded by steep mountain slopes and is categorized as an icefall glacier with two ice falls. In the uppermost part of the glacier, below the ice falls, the glacier surface is steep, but below the icefalls the surface inclination is around 85/

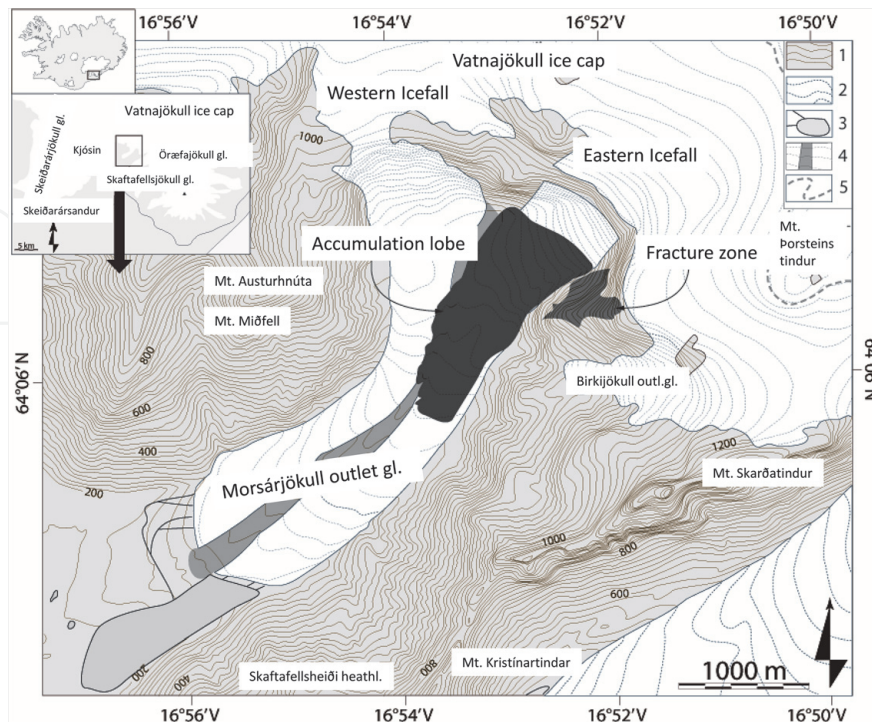


Figure 2. Location map of the Morsárjökull outlet glacier in SE Iceland. The fracture zone and the accumulation lobe marked with gray color. Legend: (1) 20 m contour lines on land, (2) 20 m contour lines on glacier, (3) proglacial lake, (4) medial moraine, and (5) equilibrium line (ELA).

1000 m. A proglacial glacier lake occurs in front of the eastern side of the glacier snout. The lake, which is today around 1.8 km long and 350–400 m wide, begun to form around 1945. This lake has increased considerably in size during the last decades. About 1.6 to 1.8 km from the glacier snout, a system of end moraines occurs crossing the valley floor, marking the maximum extent of the glacier around 1910. The glacier is drained by the Morsá Glacier River, which merged into the old Skeiðará River gorge approximately 12–13 km down glacier.

It is believed that the rock avalanche fell in two separate stages; the main part fell on March 20 and the second and smaller one on April 17, 2007. In both instances surface tremors were detected on seismographs, and on April 17 workers at the Skeiðarársandur sandur plain heard a rumbling noise from the glacier.

The rock avalanche was initiated from the north face of the headwall above the uppermost part of the glacier (**Figure 3**). The scar in the rock-face is around 330 m high, reaching from about 620 m up to 950 m and about 480 m wide on average, showing that the main part of the headwall collapsed. From a digital elevation model of the headwall, based on aerial photographs from 2003 and 2007, the total volume of debris is estimated to be around 4 to 4.5 million m³ or about 10–12 million tons. The rock avalanche debris fell first straight onto the glacier and then turned 90° downward. No indication of any deformation or erosion of the glacier surface was observed, which is similar to the description of the rock avalanche which fell on the Sherman glacier in Alaska in 1964 [20, 21].

6.2.2 Properties and data

The accumulation lobe is on average 1,5 km long, with a maximum length of 1.6 km, reaching from 520 m a.s.l. down to about 350 m a.s.l. Its width is from 125 m to 650 m or on average 480 m. The total area which the lobe covers is about 720.000 m² which was approximately 1/5 of the glacier surface in 2007. The thickness of the debris lobe was measured more than 8 m in places, but its mean thickness was somewhere between 5.5 and 6.2 m. In 2007 the debris mass is coarse-grained and boulder-rich with little fine material. Blocks over 5 to 8 m in diameter are common on the edges of the lobe up to 1.6 km from the source. The largest block which was observed in the accumulation lobe is around 800 tons located on the western side of



Figure 3.

The headwall above the eastern icefall in the uppermost part of the Morsárjökull outlet glacier and the accumulation lobe (Photo Þorsteinn Sæmundsson 2007).

the debris lobe, approximately 800 m from the scar. On the surface of the accumulation lobe flow line structures and longitudinal ridges, up to 3–4 m high were observed. Similar phenomena have been described from other rock avalanches on glaciers, e.g., the Sherman glacier in Alaska [21] and the Little Tahoma Peak glacier in the Washington state [22].

It is evident that the Morsárjökull glacier has retreated considerably during the last century, and during the last decade, the melting has been very rapid. Therefore, it is thought that undercutting of the mountain slope by glacial erosion and the retreat of the glacier are the main contributing factors leading to the rock avalanche. The glacial erosion has destabilized the slope, which is chiefly composed of palagonite and dolerite rocks, affected by geothermal alteration. Hence a subsequent fracture formation has weakened the bedrock. The exact triggering factor, however, is not known. No seismic activity or meteorological signal, which could be interpreted as triggering factors, such as heavy rainfall or intensive snowmelt, was recorded prior to the rock avalanche.

6.2.3 Evaluation

A quick calculation using (11) shows that there is very little difference between the average thickness and y_0 . The upper section is around 500 m long, making the lower section 1000 m. The glacial surface just below where the slide stops inclines by 5.6 %; this is put as $\tan\phi'$.

It is necessary to estimate the flow time of the slide in order to find the Chezy coefficient C ; this is found from a tremor recorded in a nearby earthquake station to be 100 seconds, but this estimate is very uncertain. However, it affects only c and C . **Table 2** shows the data and the calculation of the main parameters of the slide.

The main results show similar values for the upper and lower C 's. Note the large difference from the underwater slide in Case 1. Had the C values been known, the time could have been computed.

	Upper section		Lower section	
	Source	Value	Value	Dim
y_0	Data	5	7	m
θ	$\text{Arctan}(S_{f_0})$	9.0	5.1	Deg
S_{f_0}	Data	0.16	0.09	NA
S_f	$\sin\theta (1 - \tan\phi'/\tan\theta)$	0.10	0.03	NA
Time	100 totals	25	75	sec
Length	1500 total	500	1000	m
c	Length/time	20	13.3	m/s
C	$C = c / (g y_0 S_f)$	8.8	8.7	NA

Table 2.
 Upper section of the Morsárjökull slide.

6.3 Case study 3: the debris slide in the Móafellshyrna Mountain in the Tröllaskagi peninsula, central north Iceland

6.3.1 Location and event

On September 20, 2012, a large debris slide occurred at the northwest facing slope of the Móafellshyrna Mountain in the Fljótin area situated in the Tröllaskagi

peninsula, an area in central north Iceland. The local residents of the farm Prasastaðir witnessed the release of the landslide. The area was heavily eroded during the last glaciation period Iceland. **Figure 4**, modified from [15], shows the site, the location, and an aerial picture of the extent of the slide. The onset of the slide is traced to the special geology of the mountain (**Figure 4**) and thawing of permafrost in the sediments at an approximate elevation of 900 m (meters elevation above sea level) at the top of the Móafellshyrna Mountain. The thawing was proven to be the primary reason for the weakening of the sediments in the source area, but the triggering of the event was a combination of heavy rains and three earthquakes of Richter magnitude 4.2–4.5 on September 19 and 20.

6.3.2 Properties and data

The slide originates (at the headscarp) at an elevation of 880 m and runs all the way down to 330 m (**Figures 4** and 5). The total debris volume is estimated to be 312,000–480,000 m³ [15].

There are three particularly interesting problems associated with this slide. Firstly, in it are large blocks of frozen sedimentary rocks; the biggest one is 12 meters wide and 4 meters high (**Figure 6**). This large block is an integral part of the debris flow, it is carried almost halfway down the mountain, and it stops at the elevation 495–505 m and has carved an erosion channel into the mountainside, shown as black streak in the talus (rock mass at the foot of a cliff) slope in **Figure 5**, but it stops at around 500 m a.s.l.

Secondly, the massive frozen blocks inside the main debris flow will affect the flow velocity and the velocity distribution within the flow. The erosion channel

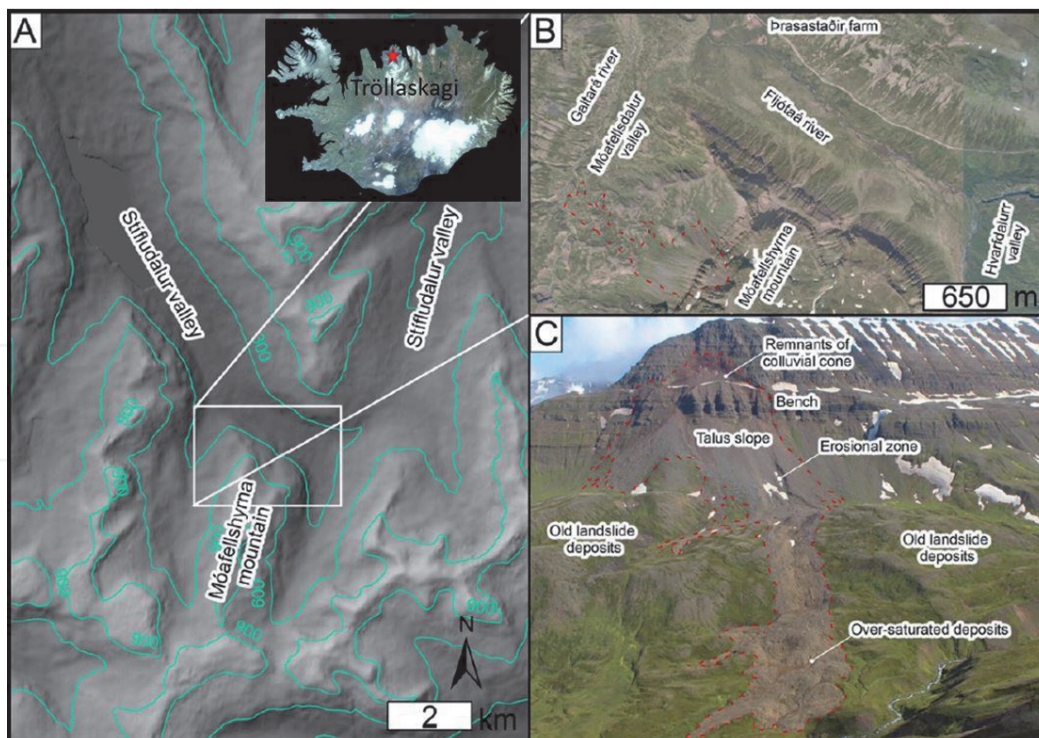


Figure 4.

The geographic setting of the Móafellshyrna site, Tröllaskagi peninsula, central northern Iceland. (A) Hillshaded digital elevation model and contours (in green, meters above sea level) of the Móafellshyrna region. Elevation data are from EU-DEM from GEMS RDA. (B) Aerial photograph of the Móafellshyrna site taken before the slide in 2012 from the website Samsyn. (C) Oblique photo of the Móafellshyrna debris slide in July 2015 taken by Costanza Morino. In panels B and C, the perimeter of the slide is marked with red dashed line taken from the trimble data for the deposits and reconstructed from photographs for the upper part; in C this line has been manually traced onto the oblique image. Modified from [15].

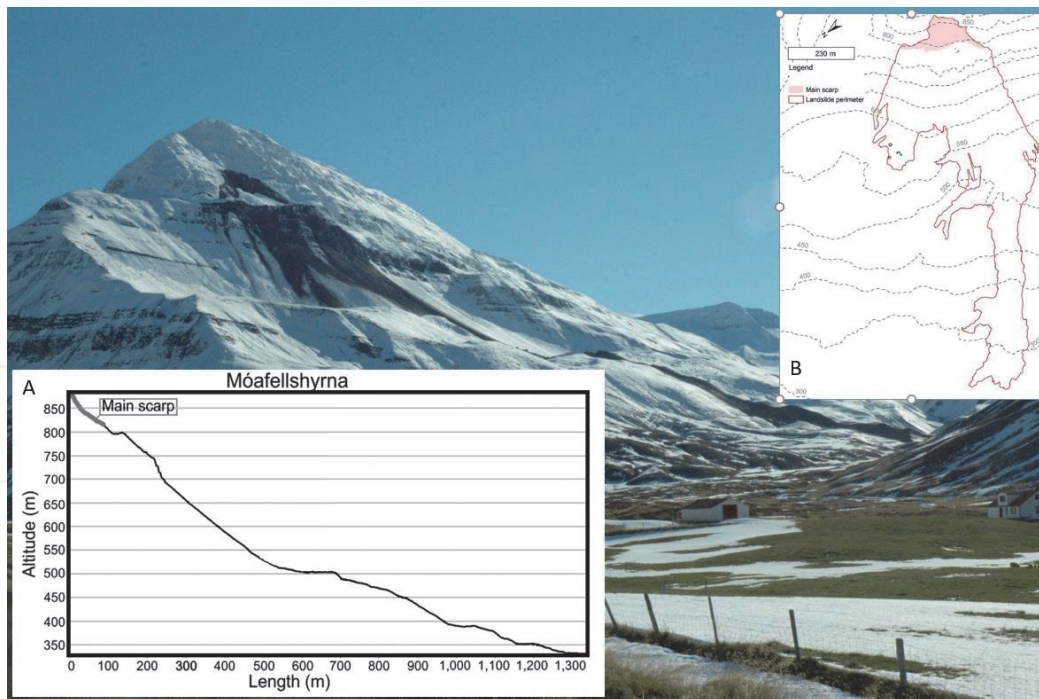


Figure 5. The Mófellshyrna landslide (photo taken few hours after the slide on September 20, 2012). (A) The topographical profile of the Mófellshyrna landslide. (B) Distribution map of the landslide (photo by Þorsteinn Sæmundsson 2012). Modified from [15, 23].



Figure 6. Landslide debris and an ice-cemented block resting at 495–505 m a.s.l. The block is around 12 m wide and 4 m high (photo by Þorsteinn Sæmundsson September 29, 2012).

shows that the part of the slide flowing in it has lower velocity than the rest of the flow, which means that the main flow is providing a part of its momentum to the blocks. This may result in a thicker slide that does not run as long out as a slide of uniform material would have done.

Thirdly, the blocks run over a 100-meter-high cliff below the source area at 690. Here they pick up momentum and carve the channel before they stop, 170 m higher up than the rest of the slide which runs about 700 meters farther out (Figure 5). The force of the flow on the blocks is unable to transport them any further in spite

of the momentum gain. This acts as flow resistance on the part of the slide flowing by and may be a significant factor in determining the flow properties downstream, e.g., that it stops where it does and does not flow any further.

Figure 5A and **B** explains the properties of this very complicated slide visually.

The following description of the slide shows where erosion and deposition occurred in the slope (**Figure 5**) [15, 23].

- The debris slide was detached from a main scarp at an elevation of 880 m a.s.l. The source material of the landslide was a colluvial cone. Part of the cones front, slides off a steep 100 m high rockwall, at around 800 m a.s.l. It is estimated that the volume of deposit which broke the frontal part of the colluvial cone was around 120,000–180,000 m³. The headscarp has an average slope of around 30–35°.
- Below the rockwall at around 700 m a.s.l., a 300-m-long, 80–100-m-wide, and 8–10-m-deep channel was carved into the 200-m-high talus slope deposits, entraining around 192,000–300,000 m³ of material. The average slope of the talus is around 30°.
- At 495–505 m a.s.l. at the foot of the talus slope, some of the landslide deposits came to a rest, where the average slope angle is less than 10°.
- The rest of the landslide material traversed down the mountain slope from 495 m and finally came to a rest at 330 m. The uppermost 100 m of the slope are steeper with an averaged slope angle of around 20–25° and in the lowermost 70 m of the slope around 10–15° angle.

6.3.3 Evaluation

The slide may be translatory from the resting position of the big block at around 500 m a.s.l. until it stops. The section around it is then the starting point of the downstream flow, and its initial conditions are the time history of the velocity and flow depth in that section.

From **Figure 5** we see that the slide stops at the bottom slope of $\tan\varphi' = 50/400 = 0,125$ or $\varphi' = 7^\circ$. The width of the slide can be approximately estimated from **Figures 4** and **5**. According to Section 6.2.2, the total flow mass to run from the talus slope from 700 to approximately 500 m a.s.l. is estimated to be 192,000–300,000 m³. This provides an estimate that the flow channels from 500 down to 330 m has an average depth of 6 m. If the flow channels are supposed to have a parabolic shape, this corresponds to 2/3 of their maximum depth. The profiles and location of these channels are shown in **Figures 5A** and **B**. By assuming the same Chezy coefficients as in **Table 2**, we can calculate **Table 3**.

The results indicate that the translatory theory can model the slide quite well. The flow velocity c is found and used to calculate the flow times from 505 to 400 m height. It takes the flow 25,5 s to reach the 330 m elevation but only 8,5 s to run from 495 to 400 m. However, it takes the total mass 28 seconds (total flow 28) to flow from 495 to 400 m. This is longer time than the run from 400 to 330 m, so some material will be left between 495 and 400 m when the downstream end stops, making some accumulation to take at that height interval.

This is an example of computing slide properties from known C values in a fast and effective manner. The velocity c in the steeper part of the lower part of the slide from 495 to 400 m is high, certainly high enough to produce the rumbling noise

	495–400 m		400–330 m	
	Source	Value	Value	Dim
y_0	2/3 of the max. value	6	6	m
Width	Figure 5B	80	130	m
θ	$\text{Arctan}(S_{f_0})$	19	10	Deg
S_{f_0}	Figure 5A	0,33	0,17	NA
S_f	$\sin\theta (1 - \tan\phi' / \tan\theta)$	0,34	0,17	NA
Time	Length/c. Total flow 28	8,5	25,5	sec
Length	Figure 5A	263	360	m
c	$c = C (g y_0 S_f)$	31	14	m/s
C	Table 2	8,8	8,7	NA

Table 3.
 Two sections in the Móafellshyrna slide.

heard in the nearby farm. The velocity from 400 to 330 m is still high; it takes a slope of 70 meters to stop it.

7. Conclusion

The translatory wave theory is an old tool from the science of hydrodynamics that can be adapted to landslides. However, it is not possible to say that it may be used for certain classes or groups of landslides in the geological classification system of landslides. The theory can be used for all slides that flow downhill with a flow governed by gravitational forces, where the slide has a wavelike front and the slide follows as a frontal wave with the same velocity.

The translatory wave equation can be modified to describe this form of a landslide by introducing a new parameter, the slope factor S_f into the flow equations as to control the excess shear force in the landslide and its relation to the actual shear strength of the flowing mass. The slope factor controls how great a part of the actual shear force is in excess of the shear strength and thereby the velocity of the flow.

The slope factor has to be assumed piecewise constant, and the flow stops when it becomes zero. This model can give a very good picture of the flow and can save valuable time and effort, when a more detailed numerical treatment is necessary.

The translatory model is used for moving slides; it cannot predict the onset of a slide. But when in motion, it can predict the length and thickness of the slide from the knowledge of the ground slope and the soil parameters, the Chezy coefficient, and the slope factor. And vice versa, for a mapped slide, it can predict the soil parameters.

There are three studied cases presented, first the famous Tohoku tsunami in Japan, which became very strong because of the earthquake that started the tsunami and a landslide that amplified the tsunami. Both Chezy's coefficient and the slope factor are found.

The second case study is a landslide down the Morsárjökull outlet glacier in Iceland, starting as a rock slide, but it turns downhill into a glacier and turns into a flow slide, in clear contrast to the Tohoku submarine slide. This slide flows first down a steep upper slope and then down a milder lower slope and then finally stops on an even milder slope with a flow factor zero. The results for the upper and lower sections show different slope factors, the lower one belonging to the lower section. The lower thickness value belongs to the upper section, but the Chezy coefficients

are similar for the two sections. There is reason to believe that further research can uncover a pattern for the Chezy coefficient for similar sites. Then runout lengths and risk area can be approximately predicted for slides of known volume, known from developing cracks or other discernable geological evidence.


The third case study is a landslide down the MÓafellshyrna Mountain in North Iceland. It has previously been shown that this slide can be modeled with the RAMS model. Here it is demonstrated that it can also be modeled using the Chezy coefficients estimated in case study 2. The possibility to keep a data set containing Chezy coefficients that can be used in future estimates is a considerable help in hazard assessments.

Author details

Jónas Elíasson* and Þorsteinn Sæmundsson
Faculty of Engineering and Natural Sciences, University of Iceland, Reykjavík,
Iceland

*Address all correspondence to: jonase@hi.is

IntechOpen

© 2019 The Author(s). Licensee IntechOpen. This chapter is distributed under the terms of the Creative Commons Attribution License (<http://creativecommons.org/licenses/by/3.0>), which permits unrestricted use, distribution, and reproduction in any medium, provided the original work is properly cited. 

References

- [1] Highland, LM, Bobrowsky P. The Landslide Handbook—A Guide to Understanding Landslides, United States Geological Survey, Landslide Program and National Landslide Information Center, Mail Stop 966, Box 25046, Denver Federal Center, Denver, Colorado, 80225 USA. 2008. Available from: <https://pubs.usgs.gov/circ/1325/>
- [2] van Westen C. Introduction to Landslides, Part 1: Types and Causes. Available from: http://www.adpc.net/casita/Course%20Modules/Landslide%20hazard%20assessment/Landslides_types_and_causes.pdf
- [3] Komac M. A landslide susceptibility model using the analytical hierarchy process method and multivariate statistics in perialpine Slovenia. *Geomorphology*. 2006;**74**(1-4):17-28
- [4] Guzzetti F, Malamud BD, Turcotte DL, Reichenbach P. Power-law correlations of landslide areas in central Italy. *Earth and Planetary Science Letters*. 2002;**195**(3-4):169-183
- [5] Casadei M, Dietrich WE, Miller NL. Testing a model for predicting the timing and location of shallow landslide initiation in soil-mantled landscapes. *Earth Surface Processes and Landforms: The Journal of the British Geomorphological Research Group*. 2003;**28**(9):925-950
- [6] Crozier MJ. Prediction of rainfall-triggered landslides: A test of the antecedent water status model. *Earth Surface Processes and Landforms*. 1999; **24**(9):825-833
- [7] Hergarten S, Neugebauer HJ. Self-organized criticality in a landslide model. *Geophysical Research Letters*. 1998;**25**(6):801-804
- [8] Borga M, Dalla Fontana G, Da Ros D, Marchi L. Shallow landslide hazard assessment using a physically based model and digital elevation data. *Environmental Geology*. 1998;**35**(2-3): 81-88
- [9] Tsai TL, Yang JC. Modeling of rainfall-triggered shallow landslide. *Environmental Geology*. 2006;**50**(4): 525-534
- [10] Farahmand A, AghaKouchak A. A satellite-based global landslide model. *Natural Hazards and Earth System Sciences*. 2013;**13**(5):1259-1267
- [11] Eliasson J, Kjaran SP, Holm SL, Gudmundsson MT, Larsen G. Large hazardous floods as translatory waves. *Environmental Modelling and Software*. 2007 Oct 1;**22**(10):1392-1399
- [12] Douglas JF, Gasiorek JM, Swaffield JA. *Fluid Mechanics*. 3rd Edn. England: Longman Scientific & Technical, Essex CM20 2JE; 1995. p. 819
- [13] McDougall S, Hungr O. A model for the analysis of rapid landslide motion across three-dimensional terrain. *Canadian Geotechnical Journal*. 2004; **41**(6):1084-1097
- [14] Eliasson J. Earthquake-generated landslides and tsunamis. In: *Earthquakes-Impact, Community Vulnerability and Resilience*. Rijeka: IntechOpen; 2019
- [15] Sæmundsson P, Morino C, Helgason JK, Conway SJ, Pétursson HG, Barceló D, et al. The triggering factors of the Móafellshyrna debris slide in northern Iceland: Intense precipitation, earthquake activity and thawing of mountain permafrost. In: Barceló D, Gan J, editors. *Science of the Total Environment*. 2018;**621**:1163-1175
- [16] JAMSTEC. Causal Mechanisms of Large Slip during the Tohoku Earthquake of 2011. Revealed through

Hydraulic Analysis of Fault Drilling Samples from the Deep-Sea Scientific Drilling Vessel Chikyu; Japan Agency for Marine-Earth Science and Technology. 2013. Available from: http://www.jamstec.go.jp/e/about/press_release/20131008/

[17] Land and Sea Areas of Crustal Movement and Slip Distribution Model of the Tohoku-Pacific Ocean Earthquake: Coseismic Slip Distribution Model. Report by the Geographical Survey Institute, Japan. 2011. Available from: <http://www.gsi.go.jp/cais/topic110520-index-e.html>

[18] Fujii Y, Satake K, Sakai SI, Shinohara M, Kanazawa T. Tsunami Earthquakes - Impact, Community Vulnerability and Resilience source of the 2011 off the Pacific coast of Tohoku earthquake. *Earth, Planets and Space*. 2011;**63**(7):55

[19] Sæmundsson Þ, Sigurðsson IA, Pétursson HG, Jónsson HP, Decaulne A, Roberts MJ, et al. Bergflóðið sem féll á Morsárjökul 20. mars 2007 –hverjar hafa afleiðingar þess orðið? *Náttúrufræðingurinn*. 2011;**81**(3–4): 131-141 (in Icelandic)

[20] Post AS. Alaskan Glaciers: recent observations in respect to the earthquake-advance theory. *Science*. 1965;**148**:366-368

[21] Shreve RL. Sherman landslide, Alaska. *Science*. 1966;**154**(3757): 1639-1643

[22] Fahnstock RK. Little Tahoma Peak rockfalls and avalanches, Mount Rainier, Washington, USA. In: Voight B, editor. *Developments in Geotechnical Engineering*. Vol. 14. Part A. New York: Elsevier; 1978. pp. 181-196

[23] Morino C, Conway SJ, Sæmundsson Þ, Helgason JK, Hiller J, Butcher FEG, et al. Molards as an indicator of permafrost degradation and landslide processes. *Earth and Planetary Science Letters*. 2019;**516**:136-147